Geomech. Geophys. Geo-energ. Geo-resour. (2022) 8:210
https://doi.org/10.1007/s40948-022-00519-7

ORIGINAL ARTICLE

Pore morphology effect on elastic and fluid flow properties in Bakken formation using rock physics modeling

Ogochukwu Ozotta · Mohammad Reza Saberi · Oladoyin Kolawole · Mohamed Lamine Malki · Vamegh Rasouli · Hui Pu

Received: 1 March 2022 / Accepted: 6 November 2022 / Published online: 28 November 2022
© The Author(s) 2022

Abstract Unconventional geo-resources are critical due to their important contributions to energy production. In this energy transition and sustainability era, there is an increased focus on CO_2-enhanced oil recovery (CO_2-EOR) and geological CO_2 storage (GCS) in unconventional hydrocarbon reservoirs, and the extraction of hot fluid for energy through enhanced geothermal systems. However, these energy solutions can only be achieved through efficient stimulation to develop a complex fracture network and pore structure in the host rocks to extract heat and hydrocarbon, or for CO_2 storage. Using Bakken formation well data and rock physics models, this study aimed to identify the post-depositional effect of pore structure on seismic velocity, elastic moduli, and formation fluid; and further predict the best lithofacies interval for well landing, and the implications for fluid (gas, oil, and water) recovery in naturally- and often systematically-fractured geosystems. The KT and DEM models' predictions show distinct formation intervals exhibiting needle-like pores and having higher seismic velocities (V_p and V_s) and elastic moduli (K and μ), relative to other formation intervals that exhibit moldic pores. At the same fluid concentration, the needle-like pores (small aspect ratios) have a higher impact on elastic moduli, V_p, and V_s than on the moldic spherical pores with all other parameters held constant. V_p is affected more than V_s by the properties of the saturating fluid (gas, oil, or water) with V_p being greater in Bakken formation when it is water-saturated than when it is gas-saturated. V_s exhibit the reverse behavior, with V_s greater in the gas-saturated case than in the water-saturated case. Further, analyses suggest that the middle Bakken formation will have a higher susceptibility to fracturing and faulting, and hence will achieve greater fluid (oil and water) recovery. Our findings in this study provide insights that are relevant for fluid production and geo-storage in unconventional reservoirs.

Supplementary Information The online version contains supplementary material available at https://doi.org/10.1007/s40948-022-00519-7.

O. Ozotta (✉) · H. Pu
Department of Petroleum Engineering, University of North Dakota, Grand Forks, ND 58202, USA
e-mail: ogochukwu.ozotta@und.edu

M. R. Saberi
Geosoftware, 2591 XR The Hague, Netherlands

O. Kolawole (✉)
John A. Reif, Jr. Department of Civil and Environmental Engineering, New Jersey Institute of Technology, Newark, NJ 07102, USA
e-mail: oladoyin.kolawole@njit.edu

M. L. Malki · V. Rasouli
Department of Petroleum Engineering, University of Wyoming, Laramie, WY 82071, USA

Article highlights

- Integrated well log data and rock physics models.
- Investigated the effect of changes in pore structure on elastic properties and fluid flow in shale.

- Increase in porosity causes a reduction in elastic moduli and seismic velocities.
- V_p is more affected by pore geometry than V_s depending on density and properties of saturating fluid.
- Lithofacies with needle−like pores are more susceptible to fracturing than lithofacies with intragranular pores.

Keywords Rock physics · Fracture mechanics · Pore geometry · Aspect ratio · Shale rock physics

List of symbols

V_p	Compressional velocity
V_s	Shear velocity
ρ	Density
M_{VRH}	Modulus of Voigt, Reuss and Hill average
M_V	Voigt upper bound
M_R	Reuss lower bound
f_i	Volume fraction used to compose the rock constituent minerals
M_j	Modulus of the *i*th component
M	Shear modulus or the bulk modulus.
K_{KT}	The effective bulk modulus of Kuster−Toksöz
μ_{KT}	The effective shear modulus of Kuster−Toksöz
k_s	Bulk modulus of the matrix
K_{dry}	Effective bulk modulus of dry rock
K_{sat}	Effective bulk modulus of saturate rock
K_0	Effective bulk modulus of the mineral material
k_{fl}	Effective bulk modulus of the pore fluid
m_s	Modulus of the inclusion
G_{dry}	Effective shear modulus of dry rock
G_{sat}	Effective shear modulus of the pore fluid
K_i	Bulk modulus of inclusion
K_{fl}	Bulk modulus of saturating fluid
α	Aspect ratio
y	Porosity
μ_s	Shear modulus of the matrix
μ_i	Shear modulus of inclusion
K^*_{DEM}	Bulk moduli of the matrix of phase
K_2	Bulk moduli of the matrix of phase 2
$K^*_{DEM}(y)$	Effective bulk moduli of DEM
μ^*_{DEM}	Shear moduli of the matrix of phase 1
μ_2	Shear moduli of the matrix of phase 2
$\mu^*_{DEM}(y)$	Effective shear moduli of DEM
P and Q	The geometry factor for inclusion of material 2 in a background medium
P^{si} and Q^{si}	The geometry factors
ς_s	$\frac{\mu}{6}\frac{(9K+8\mu)}{(K+2\mu)}$

1 Introduction

Unconventional reservoirs are a critical resource in this era of energy transition and sustainability due to their important contributions to energy production and geo-storage. Currently, there is an increased focus on CO2-enhanced oil recovery (CO_2-EOR) (Welkenhuyse et al. 2018; Wei et al. 2021; Kashkooli et al. 2022) and geological CO_2 storage (GCS) (Eshkalak and Aybar 2015; Senger et al. 2015; Levine et al. 2016; Azenkeng et al. 2020; Kolawole et al. 2021a, 2022; Ozotta et al. 2021a, b, c) in unconventional hydrocarbon reservoirs, and the extraction of hot fluid for energy through enhanced geothermal systems (Gholizadeh Doonechaly et al. 2013; McClure and Horne 2014; Kolawole et al. 2021b). These energy solutions can only be achieved through efficient stimulation to develop a complex fracture network and pore structure in the host rocks to extract heat and hydrocarbon, or for CO_2 storage. The linkage of hydraulic fractures and pre-existing natural fractures are important mechanisms for fracture network connectivity and pore structure enhancement.

The distinctive ultra-low porosity and permeability of an unconventional reservoir, as seen in the Bakken Formation in the Williston Basin, North Dakota, is the main obstacle to fluid recovery and production from the reservoir (Sorensen et al. 2014). Without the enhancement of such hydrocarbon reservoirs via hydraulic stimulation to improve the porosity and permeability of the reservoir and improve its hydrocarbon recovery, unconventional reservoirs cannot be produced economically (McGlade et al. 2013; Wang et al. 2014). Here, identifying the mechanisms of the pore structure of the reservoir formation is crucial since they can impact seismic velocities (V_p and V_s), and fracture initiation and propagation. Previous research works have already investigated how pore morphology affects the seismic velocities of rocks and composite geomaterials (Levin et al. 2004; Markov et al. 2006; Paoletti 2012; Candikia et al. 2017; Handoyo et al. 2019; Kolawole and Ispas

2019; Mavko et al. 2020; Kolawole 2022). The findings from these investigations demonstrate that when porosity is held constant, cracks (low aspect ratio) dramatically reduce seismic velocities more than spherical pores (high aspect ratio). This shows that compressional and shear velocities play a part in the fracturing of rocks because their low values indicate regions that are more prone to fracturing and faulting (Paoletti 2012). Therefore, analyzing and modeling seismic velocities can enhance hydraulic fracturing and stimulation operations.

Rock physics templates (RPTs) have been developed for sandstone reservoirs (Avseth et al. 2000, 2010; Singha and Chatterjee 2017) and carbonate reservoirs (Yu et al. 2014; Hilman and Winardhi 2019) to guide seismic inversion interpretation results for reservoir characterization and fluid identification, but no RPT for an unconventional reservoir with a blend of siliciclastic and carbonate rock has been developed. For sandstone reservoir, rock physics models like the constant cement model (Avseth et al. 2000), the contact cement model (Dvorkin et al. 1996), and the friable sand model (Dvorkin and Nur 1996) has been developed. For carbonate rocks, the pores are often modeled as the ideal ellipsoid inclusions ($\alpha < 1$) using an effective medium inclusion—based model, such as Kuster and Toksöz (KT) model (Kuster and Toksöz 1974), Differential Equation Medium (DEM) (Norris 1985) and self—consistent approximation (SCA) (Berryman 1980a, b). Here, the most important parameter to be defined is the pore geometry. When a fluid-filled porous medium is a composite of two porous phases, each of which could be described separately by the more conventional Gassmann relations. The generalized Gassmann's equation describes the static or low-frequency effective bulk modulus of the porous medium (Berryman and Milton 1991). This is an improvement over the standard Gassmann equation, which assumes a single, statistically homogeneous porous constituent with a single pore-space stiffness and a single solid mineral in the porous medium. The generalized Gassmann formulation is independent of pore geometry like Gassmann's equation (Mavko et al. 2020).

Therefore, for modeling pore geometry variations in carbonate rocks using inclusion-based models, we should assume rock as an elastic matrix including certain inclusions with changing pore aspect ratios. Yan et al. (2002) showed that elastic moduli have a non-linear behavior when pore aspect ratios change. This demonstrates the problem of utilizing fixed pore aspect ratios for lithology uniformity over small depth intervals. Therefore, defining a variable pore aspect ratio is needed to have a better estimation of rock stiffness and velocities. The 'velocity deviation' term developed by Anselmetti and Eberli (1999) is a regularly used assumption for modeling pore structure effects on acoustic characteristics in carbonates (Kumar and Han 2005; Saberi 2020). Velocity deviation is defined as the differences between the measured velocities and the time-average equation of Wyllie et al (1956). This quantitative method identifies intervals with strong positive deviations (stiff pores) while interparticle and micro-porosities (weak pores) make almost zero or negative deviations (Wyllie et al. 1956). Then, the P- and S-wave velocities (V_p and V_s) are computed based on the characteristics of the mineral skeleton in relation to porosity.

The complexity of unconventional reservoir pore structures and related sensitivity to pressure and temperature changes bring more challenges and uncertainties to their elastic modeling. These uncertainties may give overestimated, underestimated, or even accurate elastic changes due to different fluids based on the reservoir pore system. Pore geometries are a significant characteristic that must be taken into account when determining elastic moduli using any theoretical effective medium models since the presence of different pore structures modify the effective elastic properties of the rock frame (Kumar and Han 2005). Intergranular, intragranular, moldic, cement dissolution, and fracture pore types are the most prevalent in unconventional reservoirs like the middle Bakken component, according to Ulmer-Scholle et al. (2014). Therefore, the key parameters in unconventional reservoir petrophysical modeling are to account for the lithofacies, pore size, and pore geometry. The middle member of the Bakken Formation exhibits significant differences in pore structure, pore distribution, and pore morphology as a result of the complex variations in its lithofacies. These variations also affect the framework's mineralogical composition, texture, porosity, and permeability. Such a heterogeneous interbedded reservoir like the middle member of the Bakken Formation requires rock physics modeling study to model its multiple pore morphology present.

Using Middle Bakken as a case study and rock physics models, the study aims to identify the post-depositional effect of pore structure on seismic velocity, elastic moduli, and formation fluid; and further predict the best lithofacies interval for lateral and vertical well landing, and its implications for fluid (gas, oil, and water) recovery in naturally- and often systematically-fractured geosystems. Firstly, the measured logs will be integrated with the pore structure evaluation to assess how geometry interpretation of the pore structure of the formation may affect the seismic wave velocity of the formation, and the significance of this factor in fracture mechanical behavior and model predictions. These data raise the following questions: (1) what influence do pore morphologies and reservoir fluid saturation have on V_p and V_s?; (2) can we deduce the pore geometry and fluid saturation phase from the seismic velocities (V_p and V_s)?; and (3) Is it possible to estimate V_p and V_s in reservoir environments given these rock physics models, and can seismic data be used to determine the saturating fluid?. Subsequently, we will use the differential effective medium (DEM) and Kuster – Toksòz (KT) model to predict V_p and V_s, and finally, we will apply fluid substitution using the Gassmann model.

2 The geologic background of the Bakken formation

As shown in Fig. 1, the upper, middle, and lower members make up the three distinct members of the Bakken formation. The upper and lower members are black, rich in organic matter, and are well-known as the source rock of the Bakken.

The Bakken formation has permeability values ranging from 0.01 to 20 mD. The middle Bakken member, which mostly consists of sandstones and siltstones but also has low porosity (1–15%) and low permeability (0.01–109 mD), it's the principal hydrocarbon-producing member, particularly for a reservoir formation (LeFever et al. 1992; Pitman et al. 2001; Nordeng and Helms 2010; Nojabaei et al. 2016; Liu and Ostadhassan 2017).

The middle Bakken member lithology are different throughout the Williston basin (North Dakota) and is made up of 7 unique lithofacies with a maximum thickness of 87 feet (LeFever et al. 1992; Pitman et al. 2001). Clastic shales, silts, sandstones, and carbonates are some of the several types of lithology (LeFever et al. 1992; Nordeng and Helms 2010). Shale, dolostones, and limestones rich in silts, sand, and oolites may be found in smaller proportions (LeFever et al. 1992). The cementations in the middle Bakken formation include calcite, pyrite, dolomite, and some light- to medium-gray cementations with bioturbation are common within the formation. The middle Bakken member fossils include articulate and less frequently inarticulate brachiopods, pelmatozoan pieces, gastropods, and numerous trace fossils.

In brief, the middle member lithofacies unit in descending order adopted from LeFever et al. (1992): (1) lithofacies unit 7 are massive to wispy laminated argillaceous siltstone, and generally cemented with calcite and dolomite. There are fossilized brachiopods, bryozoan remains, and crinoid fragments. Pyrite partially or entirely replaces fossils; (2) lithofacies unit 6 are an alternating sequence of siltstone, claystone to shale, very fine-grained sandstone, siltstone, and sandstone bed that commonly display planar or cross-ripple laminations and cemented with dolomite; (3) lithofacies unit 5 are an alternating sequence of argillaceous siltstone, very fine-grained sandstone, and shale. Parallel or slightly undulatory thin lamination with cemented dolomite, small folds, and faults from post-lithification within; (4) lithofacies unit 4 are argillaceous to sandy siltstones, very fine-grained sandstone, and local claystone with irregular and wavy lamination. Pyrite fills intergranular pores and dolomite cements them; (5) lithofacies unit 3 is composed of very fine- to fine-grained sandstone strata. The alternation of thickly laminated cross-bedded, and enormous beds. Cemented with calcite and occasionally by pyrite; (6) lithofacies unit 2 are argillaceous siltstone or sandy siltstone to very fine-grained sandstone, with small-scale clay drapes, burrows filled with pyrite, scattered crinoids, and brachiopod fossils; (7) lithofacies unit 1 are argillaceous siltstone, cemented with calcite and scattered pyrite nodules and with crinoids and brachiopods fossils intergranular porosity.

3 Method and data

3.1 Well data

As a result, the demonstration of rock physics modeling and development of RPT of unconventional

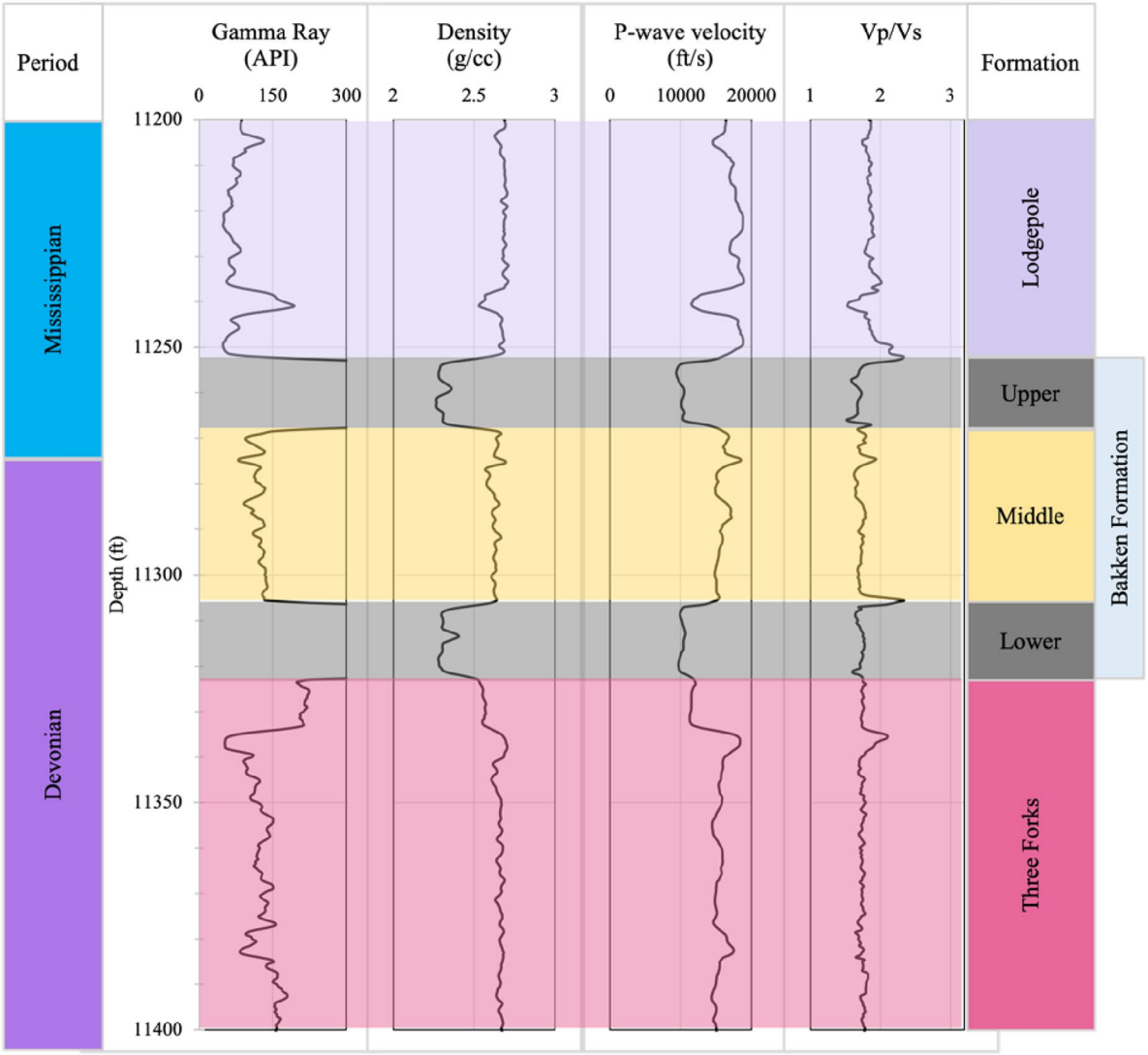

Fig. 1 Stratigraphic column of the petroleum source rocks and the reservoir in Williston Basin from well B

reservoirs in the Williston basin will be relevant for seismic AVO (amplitude variation with offset) inversion, fluid type identification, and substitution model generation. We are limited to seismic data for the field investigations in Williston Basin, and as such it is difficult to acquire spatial control over rock physics without seismic data, hence the rock physics modeling example is based only on well log data. Well logs namely, gamma-ray, resistivity, density, neutron, P-wave, and S-wave velocities are considered from two wells located in the North Fork and Little Knife fields of the basin (Fig. 2).

3.2 Rock sample preparation

Rock samples from the upper and lower members of the Bakken Formation (source rocks) were retrieved from cores stored in the North Dakota Geological

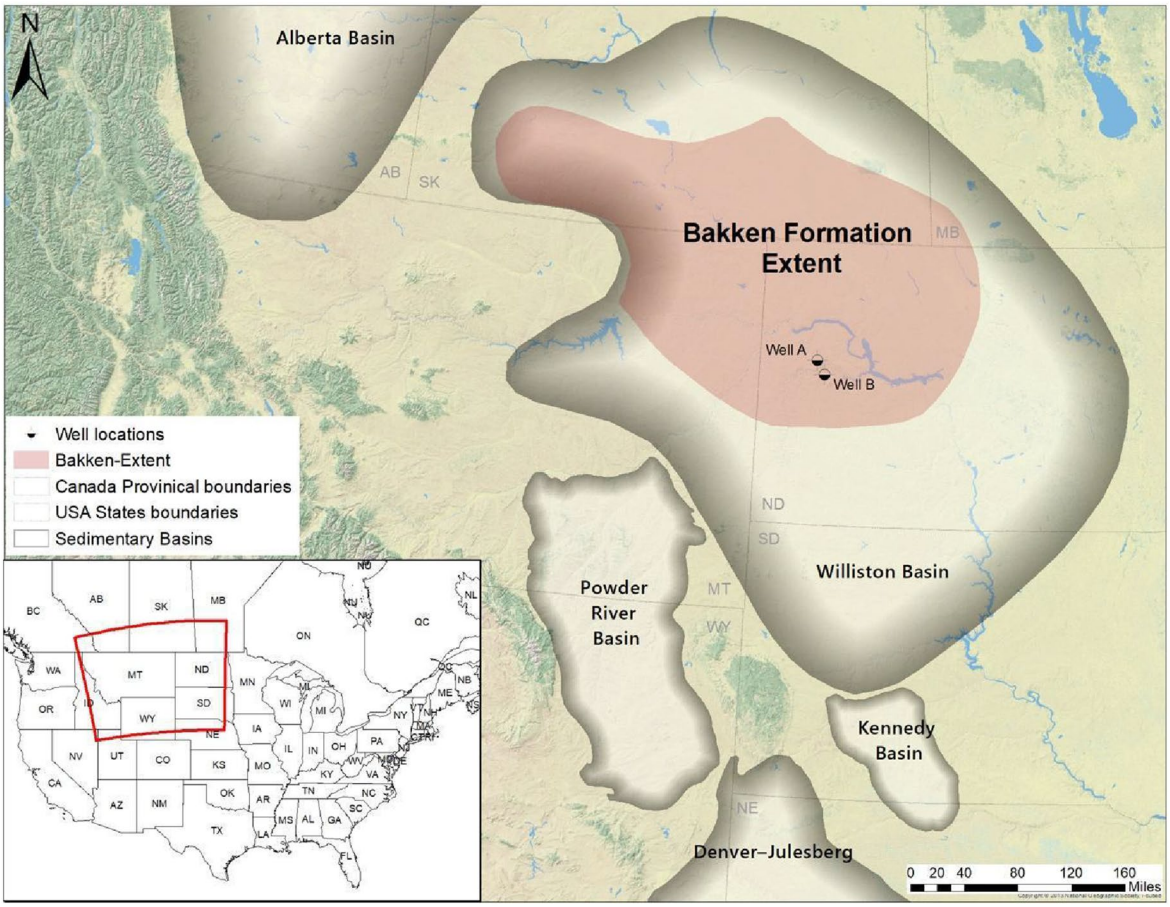

Fig. 2 Location of the wells, areal extent of the Bakken Formation and Williston Basin in United States and Canada

Survey Core Library at the University of North Dakota. The samples were dried, crushed, and sieved with < 250 µm mesh for homogenization.

3.3 Mineralogical composition

To evaluate the mineralogical components of the reservoir, the samples were crushed to a size less than 0.125 mm using a 125 mesh. For the mineralogical content analysis, a D8 advanced X-ray diffractometer (XRD) was used with a scanning rate of 3°/min in the range of 3°–90°. A curve-fitting method was used to delineate major minerals (major peaks) that exist in the spectrum.

3.4 Voigt–Reuss–Hill average moduli model

As the foremost step, the Voigt–Reuss–Hill (VRH) average method is adopted to create the matrix or background. The Voigt upper bound and the Reuss lower bound are averaged mathematically to produce the VRH average. According to Mavko et al. (2020), the relationship is shown as follows:

$$M_{VRH} = \frac{M_V + M_R}{2} \tag{1}$$

where

$$M_V = \sum_{i=1}^{N} f_i M_i; \frac{1}{M_R} = \sum_{i=1}^{N} \frac{f_i}{M_i} \tag{2}$$

To estimate the effective elastic moduli of rock in terms of its constituents, the Voigt–Reuss–Hill average is commonly used (Man and Huang 2011; Mavko et al. 2020). The input parameters for the matrix mixture are the volume fraction of the minerals, density, bulk and shear moduli, and mineral composition.

Table 1 The Middle Bakken input data for the mineral mixing using the Voigt–Reuss–Hill (VRH) model

Minerals	Density, ρ (g/cm^3)	Bulk modulus, K (GPa)	Shear moduli, μ (GPa)	Volume fraction (f)
Quartz	2.65	36.6	45.0	0.39
Pyrite	5.02	158.0	149.0	0.09
K-Feldspar	2.62	37.0	15.0	0.14
Calcite	2.71	76.8	32.0	0.16
Dolomite	2.87	94.7	45.0	0.17
Halite	2.16	24.8	14.9	0.04

Table 1 displays the values of these variables for the Middle Bakken. Following that, the resulting compressional modulus, shear modulus, and density are used as reservoir characterization input parameters. VRH assumes the rock is isotropic and the result is a heuristic, which can be useful and can accurately estimate the rock properties (Mavko et al. 2020).

3.5 Kuster−Toksoz (KT) model

In the subsurface, where rocks are typically saturated or partially saturated by fluids, seismic waves travel through two-phase media. For theoretical study, Kuster and Toksoz derived the first-order, and the long-wavelength scattering formulas for P- and S-wave velocities. This technique is one of the popular rock physics models used to calculate a medium's elastic characteristic. For various inclusion forms, the formulae for the effective moduli K_{KT} and m_{KT} Eqs. 3 and 4 respectively can be expressed as (Toksöz et al. 1976; Vernik 2016; Candikia et al. 2017; Saxena et al. 2018; Mavko et al. 2020):

$$K_{KT} = \left[k_s + f \cdot \frac{\frac{4}{3} \cdot m_s \cdot \left(k_{fl} - k_s\right)}{k_s + \frac{4}{3} \cdot m_s} \cdot P^{si}\right] \cdot \left[1 - f \cdot \frac{\left(k_{fl} - k_s\right)}{k_s + \frac{4}{3} \cdot m_s} \cdot P^{si}\right]^{-1} \tag{3}$$

$$\mu_{KT} = m_s \cdot \left[1 - f \cdot Q^{si} \frac{V_s}{m_s + V_s}\right] \cdot \left[1 + f \cdot Q^{si} \cdot \frac{m_s}{m_s + V_s}\right]^{-1} \tag{4}$$

where

$$\beta_s = \mu \cdot \frac{3 \cdot k_s + \mu_s}{3 \cdot k_s + 4 \cdot \mu_s} \tag{5}$$

And

$$V_s = \frac{\mu_s}{6} \cdot \frac{9 \cdot k_s + 8 \cdot \mu_s}{k_s + 2 \cdot \mu_s} \tag{6}$$

Pores of different shapes are found in a typical rock. The pores range in size from moldic to extremely flat, needle-like shape. The KT model represents them as a set of spheroids with various aspect ratios. KT model assumes isotropic, linear, and elastic media; limited to dilute concentrations of the inclusions; and assumes idealized ellipsoidal inclusion shapes (Mavko et al. 2020). While needle-like pores with a very low aspect ratio can be compared to penny cracks, the moldic pores can be compared to circular spheroids. In the case of a mixed aspect ratio like the middle Bakken member, the formula is given by Eqs. 7−10 can be generalized as:

For spheres inclusions:

$$P^{si} = \frac{k_s + \frac{4}{3} \cdot m_s}{k_i + \frac{4}{3} \cdot m_s} \tag{7}$$

$$Q^{si} = \frac{m_s + V_s}{m_i + V_s} \tag{8}$$

For penny shaped cracks:

$$P^{si} = \frac{k_{ss}}{k_i + \pi \cdot \alpha \cdot \beta_s} \tag{9}$$

$$Q^{si} = \frac{1}{5} \cdot \left[1 + \frac{8 \cdot \mu_s}{\pi \cdot \alpha \cdot \left(\mu_s + 2 \cdot \beta_s\right)} + 2.\frac{k_i + \frac{2}{3} \cdot \mu_s}{k_i + \pi \cdot \alpha \cdot \beta_s}\right] \tag{10}$$

3.6 Differential Effective Medium (DEM) model

The Kuster and Toksoz model is valid for a dilute pore volume (very low porosity) of tight formations, such as shales. However, the Differential Effective Medium (DEM) approach is often preferred for investigating the elastic characteristics of porous rock with higher porosity. The DEM theory models two-phase composites by incrementally adding inclusions of one

Table 2 Elastic properties of the reservoir fluids considered in the KT and DEM models

Pore fluid	K (GPa)	μ (GPa)	ρ (kg/m^3)
CO_2	0.049	0.00	450
Water	2.498	0.00	980
Gas	0.03	0.00	109
Oil	1.008	0.00	801

phase (phase 2) to the matrix phase. The effective moduli in the DEM approach are determined by the construction path chosen to reach the final composite. The DEM approach works by incorporating the background models with inclusions. DEM identifies one of the constituents as a host or matrix material in which inclusions of the other constituent(s) are embedded (Mavko et al. 2020). DEM assumes the rock is isotropic, linear, and elastic; idealized ellipsoidal inclusion shapes are assumed; the cracks are isolated with respect to fluid flow; and the process of incrementally adding inclusions to the matrix is a thought experiment and should not be used to provide an accurate description of true rock porosity (Mavko et al. 2020). The models are updated regularly as inclusions are added. The DEM equation will be expressed as Eqs. 11 and 12 (Mavko et al. 2020):

$$(1-y)\frac{d}{dy}\left[K^*_{DEM}(y)\right] = \left(K_2 - K^*_{DEM}\right)P^{(*2)}(y) \tag{11}$$

$$(1-y)\frac{d}{dy}\left[\mu^*_{DEM}(y)\right] = \left(\mu_2 - \mu^*_{DEM}\right)Q^{(*2)}(y) \tag{12}$$

The input parameters for the KT and DEM models are the compressional modulus, shear modulus, and density obtained from the matrix mixture (Voigt−Reuss−Hill model) and the reservoir fluids (gas, oil, CO_2, and brine) as presented in Table 2. The aspect ratio parameter considered in the KT and DEM models are 0.01, 0.05, and 0.2. The KT and DEM models are used to estimate the elastic properties of the unconventional reservoir rocks. The pore morphology can be determined using the KT and DEM models, and the compressional and shear wave velocities can be calculated based on the effective matrix moduli. The calculated V_p log from the KT and DEM models with different aspect ratios is then compared with the measured V_p log.

3.7 Gassmann's relations

In general, when a rock is subjected to an increase in compression, such as from a passing seismic wave, an increase in pore-pressure change is created, which resists the compression and so stiffens the rock. Gassmann's equation is used to calculate the fluid replacement effect and elastic modulus with varying fluid saturation and porosities ranging from zero to critical porosity (Gassmann 1951; Biot 1956; Mavko et al. 2020). The low-frequency Gassmann–Biot (Gassmann 1951; Biot 1956) theory predicts the consequent effect in saturated rock effective bulk modulus, K_{sat}, using the following equation (Mavko et al. 2020):

$$\frac{K_{sat}}{K_0 - K_{sat}} = \frac{K_{dry}}{K_0 - K_{dry}} + \frac{K_{fl}}{y\left(K_0 - K_{fl}\right)}, G_{sat} = G_{dry} \tag{13}$$

Gassmann's equation makes no assumptions on pore geometry and assumes a homogeneous mineral modulus and statistical isotropy of the pore space. Most significantly, it is only true at sufficiently low frequencies to dissipate excess pore pressures throughout the pore space (Mavko et al. 2020).

4 Results and discussion

The majority of the minerals found in the Bakken formation, with different proportions found throughout the middle Bakken member, are quartz, k-feldspar, calcite, dolomite, pyrite, and halite, according to the XRD data. The primary mineral components of the Middle Bakken formation analyzed in this study are quartz, calcite, dolomite and k-feldspar with 39%, 16%, 17% and 14% respectively. We neglected the influence on the elastic properties of the clay minerals in this study due to their insignificant percentage composition. The volume fraction of the minerals in Table 1 also conforms to the trend of mineral percentage fraction compared with XRD results from other studies in the Middle Bakken (Liu et al. 2016; Xu and Sonnenberg 2016).

4.1 Predicted fractomechanical properties from KT model

The elastic properties of gas, oil, and water-saturated rock models are studied for a given aspect ratio as a

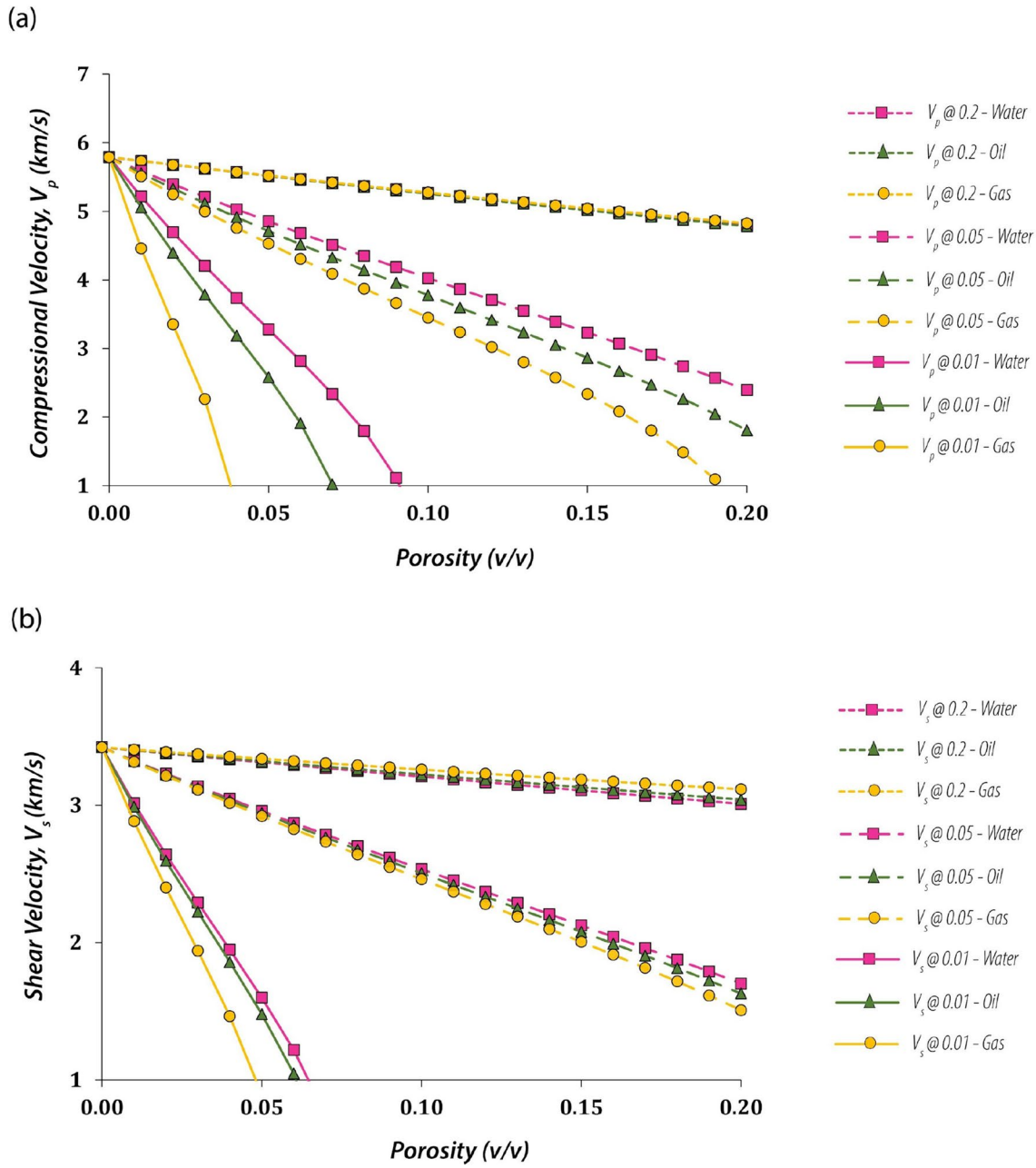

Fig. 3 KT model prediction of the effect of fluid type and pore shapes on compressional and shear wave velocities: **a** compressional wave velocity (V_p) versus porosity, and **b** shear wave velocity (V_s) versus porosity. Both relationships are presented as a function of aspect ratio represented with different markers, and the color codes and line types represent the different fluids filling the pores

function of concentration were estimated as shown in Figs. 3a, b and 4a, b for three different aspect ratios of 0.01, 0.05, and 0.2, representing cracks, intergranular, and intragranular pores respectively. Both compressional and shear velocities (V_p and V_s) are affected more by the pores with the lowest aspect ratios ($\alpha = 0.01$) than by the pores with the highest aspect ratios ($\alpha = 0.2$) where the percentage of pores

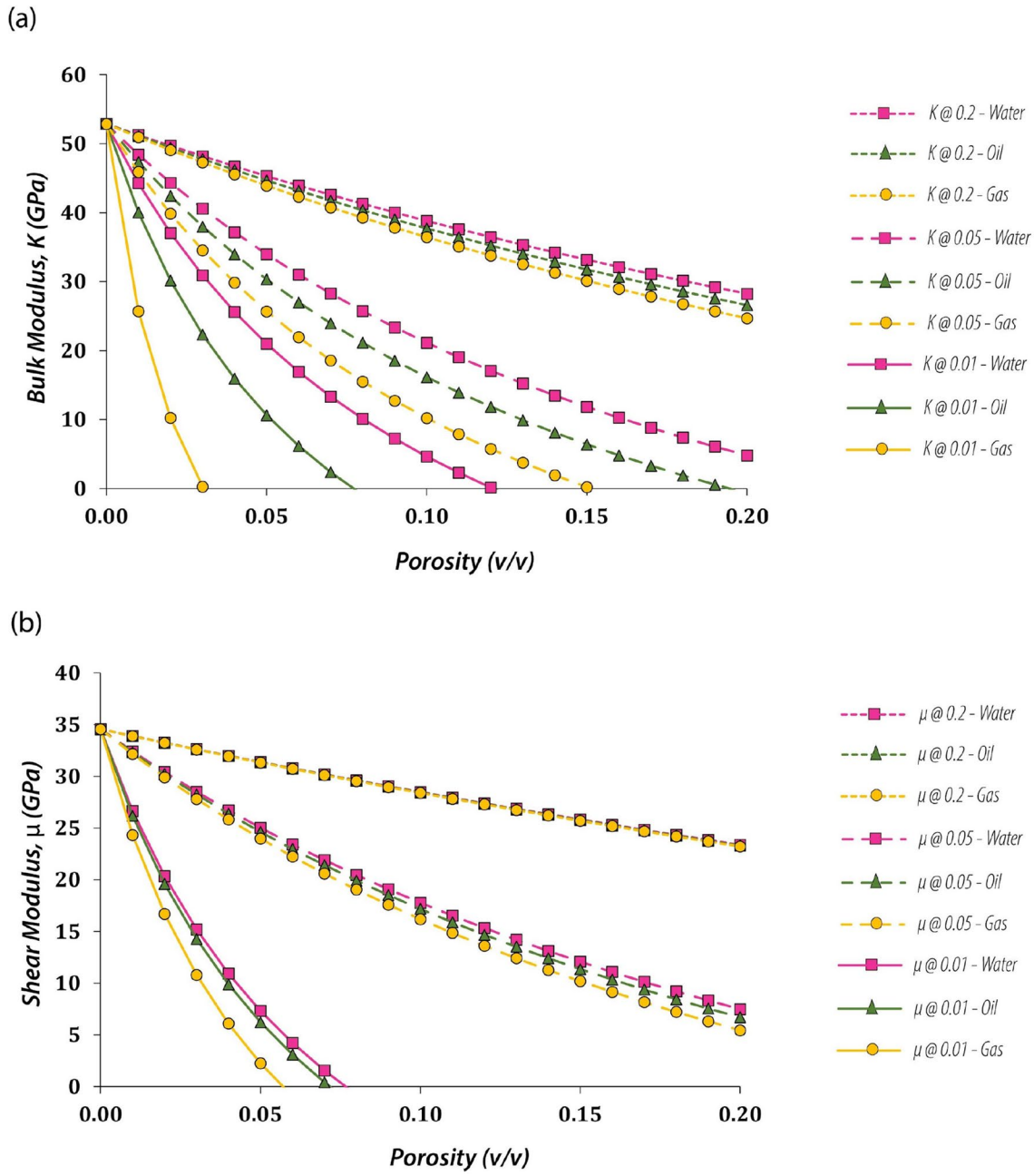

Fig. 4 KT model prediction of the effect of fluid type and pore shapes on bulk and shear moduli: **a** Bulk modulus (*K*) versus porosity, and **b** shear modulus (μ) versus porosity. Both relationships are presented as a function of aspect ratio represented with different markers, and the color codes and line types represent the different fluids filling the pores

with an aspect ratio of 0.01 reduced the velocities by about 20%. Accordingly, the rock stiffens up at higher aspect ratios while cracks and pores at lower aspect ratios are more brittle.

This is also described in Fig. 4a and b which show the stiffnesses variation with respect to different pore shapes. As pores take on a crack-like shape, both the bulk and shear moduli decrease,

with the bulk modulus being affected more so than the shear modulus.

The plots (Figs. 3a, b, 4a, b) also show that the fluid type that fills the pores also has an impact on bulk modulus, shear modulus, and velocities. Because the shear wave in fluids is insignificant as there is no shear propagation in fluids and the shear modulus stays constant as the fluid type filling the pores changes, the effect on velocities is more pronounced in V_p than in V_s. The small variation in V_s that occurs when the fluid is changed may be caused by the density characteristics of the various fluids. As a result, the figures show that the fluid type has less of an impact on velocities than the aspect ratios of the pores.

From these results (Figs. 3a, b, 4a, b), it is also shown that the fluid effect has more impact on velocities at lower aspect ratios than at higher aspect ratios, especially for gas. Figure 1 shows that at $\alpha = 0.01$, due to the substantial difference in density and bulk modulus between gas and water, where gas is, by far, more compressible than water and its density is lower, changing the fluid from water to gas causes a significant change in velocities.

The comparison of the change in V_p and V_s at different aspect ratios between oil and water shows that the impact of changing the fluid type from water to oil, or the opposite, is less significant for the elastic properties' changes. This is because these two fluids' characteristics, as compared to those of gas, are more similar to one another. The effect on rock stiffness is also demonstrated by the observations in Fig. 4a and b. Although it has been demonstrated that the pore aspect ratio decreases both compressional and shear wave velocities, the reduction is more pronounced in V_p than in V_s because shear does not capture fluids. Fluid change is more responsive to elastic properties at low aspect ratios than at large aspect ratios. This may be the result of several factors, including the fluid compressibility parameter, which affects gas more so than other fluids, and crack pores, which also permit this behavior. However, this parameter becomes less important, and the elastic properties become closer as the pore shapes tend to be circular. This phenomenon has also been observed in other studies (Toksöz et al. 1976; Levin et al. 2004; Markov et al. 2006; Candikia et al. 2017; Handoyo et al. 2019; Ozotta et al. 2021d). The uncertainties in our KT model predictions are presented in Supplementary Information (Fig. S1 and Fig. S2).

Both V_p and V_s decrease as porosity increases, and the decreasing trend is more significant at low aspect ratios than at higher aspect ratios. This phenomenon is caused by the way these pores are shaped; cracks are weaker than intragranular pores, which are known as stiff pores, and as the pore spaces increase, this stiffness difference becomes more pronounced. Regarding the susceptibility of rocks to faulting and fracture, the seismic velocities (V_p and V_s values) are extremely important (Kolawole et al. 2019, 2021b). Therefore, fracturing and faulting are strongly associated with pores that have a low aspect ratio (0.01 and 0.05). Lithofacies with a low aspect ratio are more susceptible to fracturing than lithofacies with a high aspect ratio, and this range of seismic velocities (V_p and V_s) is the target for hydraulic stimulation.

For model prediction comparison, the fluid-filling method was investigated by coupling the KT model and Gassmann fluid substitution methods. The Gassmann method underpredicts both V_p and V_s due to the assumption of interpore connectivity. This interpore connectivity was later related to KT which assumes pores to be isolated relative to the fluid transport into pores while incorporating the inclusions using KT. This variation increases with respect to the decrease in aspect ratio when the pore connectivity becomes more significant. From the analyses in Fig. 5a–d, the fluid substitution has a smaller effect when the invading fluid is gas when compared to water or oil due to its compressibility nature. Further, because Gassmann assumes that shear moduli of saturated rock are similar to dry rock, V_s is less affected by the Gassmann substitution method compared to V_p and is only affected by density change due to the addition of fluid into pores.

4.2 Predicted fractomechanical properties from DEM model

The properties affecting the curves are predominantly the pore aspect ratios (pore type) and the saturating fluid (fluid type). The penny-like (smaller aspect ratio) pores affect both the compressional and shear velocities much more than the moldic pores for a given concentration. The compressional velocities are affected more by the saturating fluids than the shear velocities. The aspect ratio of the pores affects the

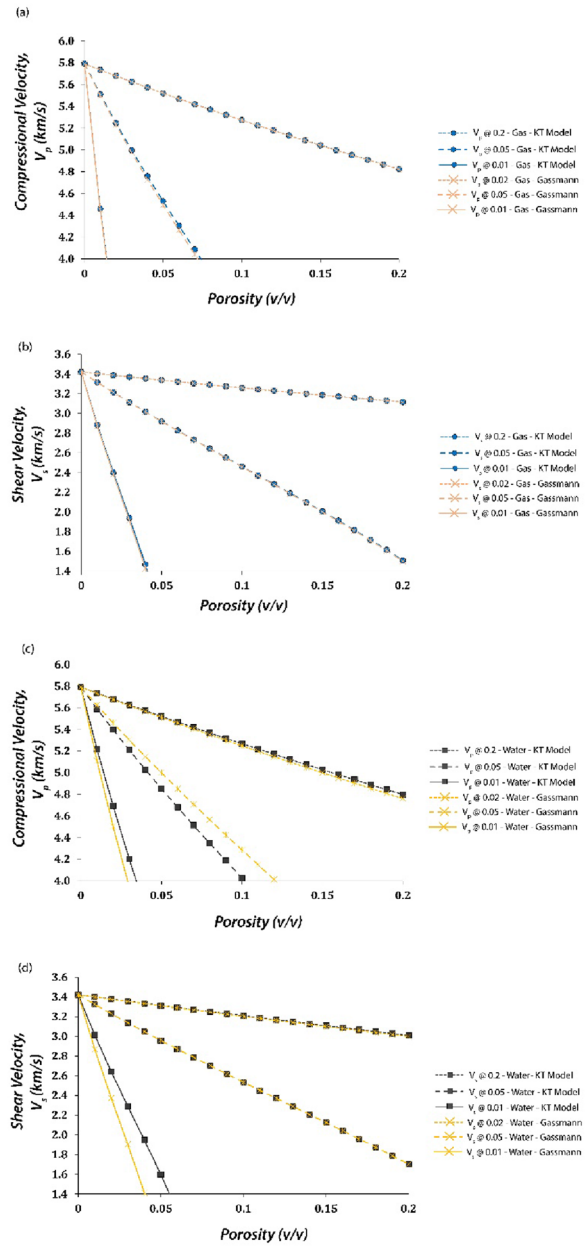

Fig. 5 KT model prediction of the effect of gas substitution method (KT versus Gassmann) on compressional and shear velocities: **a** compressional wave velocity (V_p) versus porosity, and **b** shear wave velocity (V_s) versus porosity. Both relationships are presented as a function of aspect ratio represented with different markers, and the color codes and line types represent the different fluids filling the pores

relative effects of the given reservoir fluid on compressional and shear velocities, as shown by all the cases (Fig. 6a, b). Upon gas saturation, the changes in compressional velocity are strong compared to the shear velocity. At a low aspect ratio ($\alpha = 0.01$) the change is significant but at a high aspect ratio ($\alpha = 0.2$) the change is small. This is due to the fact that the effective bulk modulus varies greatly as the saturation changes from water to gas, because the shear modulus changes very little (Fig. 7a, b). This phenomenon has also been observed in other studies (Toksöz et al. 1976; Levin et al. 2004; Markov et al. 2006; Candikia et al. 2017; Handoyo et al. 2019; Ozotta et al. 2021d). As the aspect ratio decreases, the separation increases monotonically. Because the saturant also changes the density of the composite medium, the effects of saturating fluids on velocities are much more intricate.

The V_p and V_s in moldic pores are greater when the medium is saturated with gas than when saturated

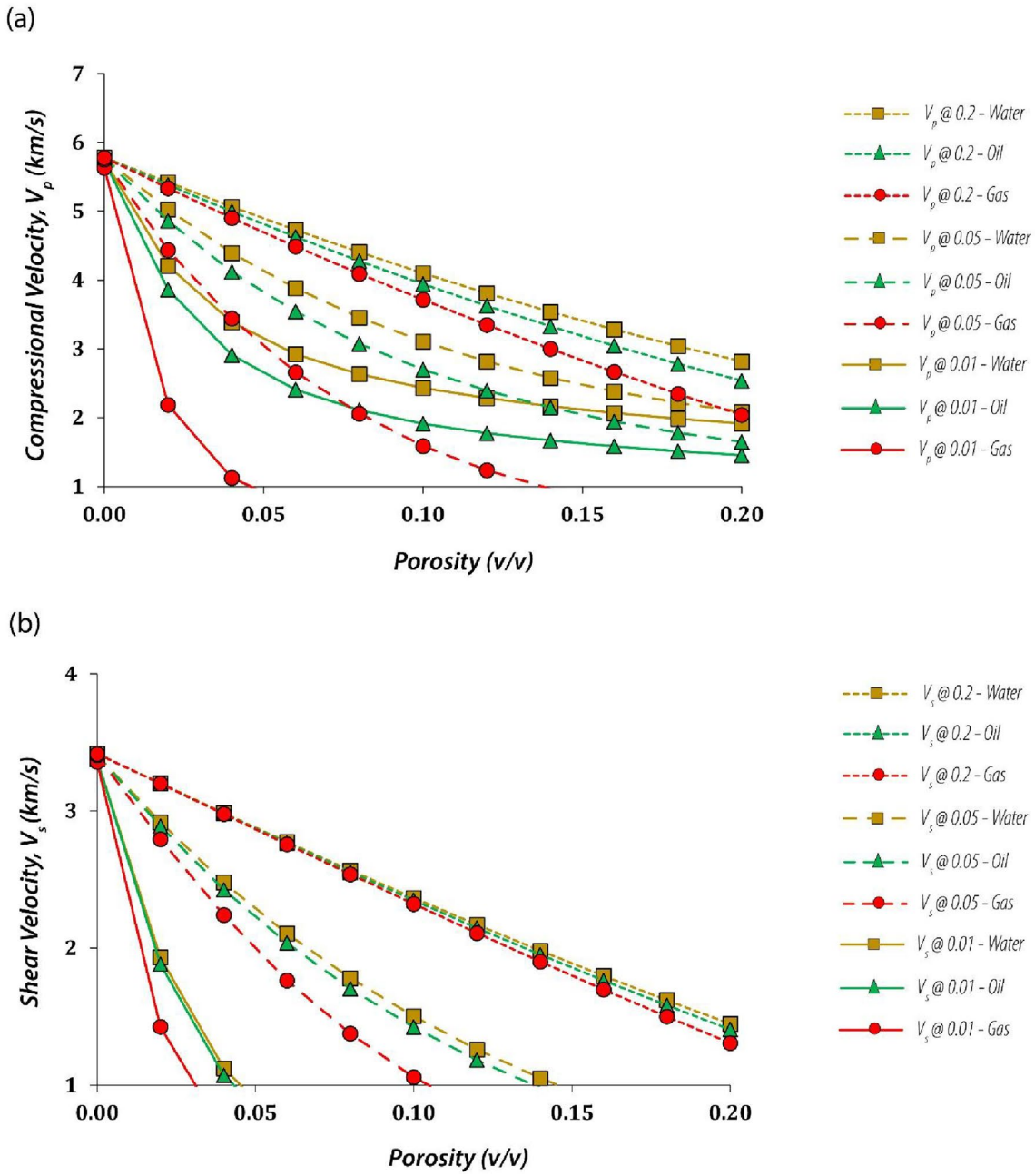

Fig. 6 DEM model prediction of the effect of fluid type and pore shapes on compressional and shear wave velocities: **a** compressional wave velocity (V_p) versus porosity, and **b** shear wave velocity (V_s) versus porosity. Both relationships are presented as a function of aspect ratio represented with different markers, and the color codes and line types represent the different fluids filling the pores

with water. This is because, with gas saturation, density drops faster than both bulk and shear moduli, resulting in greater velocities. Shear velocity is somewhat greater and compressional velocity is lower for gas saturation than for water saturation for a high aspect ratio ($\alpha = 0.2$). Both the compressional and shear velocities are lower in the gas-saturated case for small aspect ratios ($\alpha = 0.05$ and 0.01), however, the

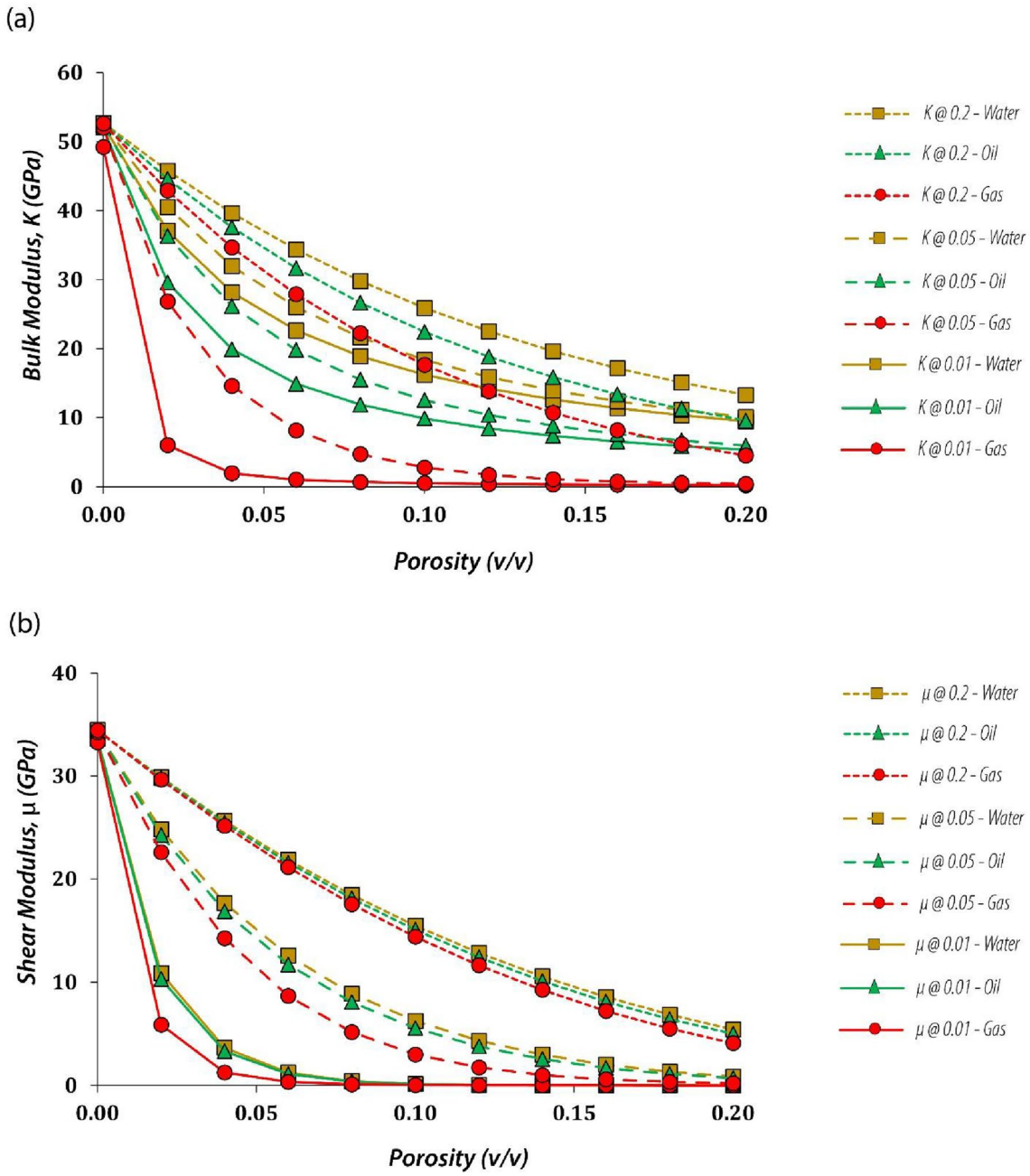

Fig. 7 DEM model prediction of the effect of fluid type and pore shapes on bulk and shear moduli: **a** Bulk modulus (*K*) versus porosity, and **b** shear modulus (μ) versus porosity. Both relationships are presented as a function of aspect ratio represented with different markers, and the color codes and line types represent the different fluids filling the pores

net difference is relatively higher for compressional velocity than in shear velocity.

Because the effective shear modulus is less sensitive to the properties of the saturating fluids, shear velocities are less impacted by saturation. The difference in gas-saturated shear velocity is caused mostly by differences in effective densities. Since compressional and shear velocities change in different directions when saturated with gas, their combined properties may be utilized to detect saturation fluids

in a reservoir. The shear modulus has a more distinct grouping of the pore types than the bulk modulus.

As with the KT model, the DEM model also has the same trend of change but the rate of change on the V_p, V_s, bulk modulus, and shear modulus is more significant in the DEM model (Figs. 6a, b, 7a, b) compared to the KT model (Figs. 3a, b, 4a, b) for all fluid types. The uncertainties in our DEM model predictions are presented in Supplementary Information (Fig. S3 and Fig. S4).

Furthermore, pore morphology interpreted the impacts of seismic wave velocity on the reservoir rock of the study area, where stiff pores or increasing aspect ratio values cause the seismic wave velocity to increase significantly and crack pores or decreasing aspect ratio values cause the seismic wave velocity to decrease significantly. According to the findings of the pore morphology modeling study, the result will define the rate at which the reservoir can be suitable for exploration (Lucia 1999; Handoyo et al. 2019). Interparticle and micro-cracks pore permeability reservoirs may significantly enhance and define the sweet spots of permeable reservoirs.

Based on the effective moduli of the reservoir, the models provided the pores morphologies and as well as the estimation of the shear wave velocity. Both models consider nearly the same parameter. However, as the procedure or method for obtaining the effective moduli differs, the outcomes of the two approaches vary. In this case, the obtained information has the same trend. To determine a better model, both models will have to be correlated with the well data to determine the model with a close match with the reservoir data.

4.3 Implications for fluid flow in Bakken formation

KT model predictions are often valid for unconventional reservoirs with very low porosity, and the DEM model predictions are often preferred for formations with higher porosity. Thus, we infer that KT and DEM predictions in this study are useful analogs that are relevant for unconventional reservoirs in other places. The KT and DEM models predicted that distinct formation intervals will exhibit needle-like pores and have higher seismic velocities (V_p and V_s) and elastic moduli (K and μ), relative to other formation intervals that exhibit moldic pores. Similarly, our analyses show that the fracture mechanical property of the reservoir rock controls the fluid circulation pathways and recovery which influences fracture nucleation and propagation.

Previous field observations, experimental, and numerical studies have demonstrated that fractures propagating from a stiff interval towards a less-stiff one tend to propagate more efficiently and commonly penetrate the contacts (Laubach et al. 2009; Gudmundsson et al. 2010; Slatt and Abousleiman 2011; Ferrill et al. 2014; Galvis et al. 2018; Kolawole et al. 2021b). These suggest that induced fractures from target lithofacies characterized by low aspect ratios, and stiffer rocks with higher bulk and shear modulus, will tend to generate a coherent and connected fracture network that can connect with other pre-existing natural fractures or reactivate faults. Therefore, in the Bakken formation used for this case study, we suggest that the middle Bakken formation has a higher susceptibility to fracturing and faulting, and hence will achieve greater fluid recovery than the upper and middle Bakken formations. Since the bulk and shear moduli are lower for the gas-saturated case than the oil or water-saturated cases for all the pore shapes investigated, our results suggest that the middle Bakken formation will have higher recovery and production of oil and water than gas.

In Gassmann (1951), which provided the original work widely applied to porous rocks, the bulk modulus of the medium depends upon the matrix bulk modulus and the frame modulus. Just the total porosity can be used to determine V_p and V_s, and elastic moduli; not the pore shape specifically. The shape effect comes in through the parameter of the total porosity. Additionally, it is assumed that the saturating fluid has no impact on the effective shear modulus. This assumption is not true for needle-like pore or cracks but hold for spherical pores (Toksöz et al. 1976).

There are certain limitations to the models used in this study. VRH, KT model, DEM and Gassmann's are limited to isotropic, linear and elastic media. KT model is limited to dilute the concentration of the inclusions. KT model and DEM assumes idealized ellipsoidal inclusion shapes. The cracks in DEM are isolated with respect to fluid flow and the process of incrementally adding inclusions in the matrix is a thought experiment. Gassmann's equation assumes a homogeneous mineral modulus and most significantly, it is only true at sufficiently low frequencies to equilibrate the produced pore pressure throughout

the pore space (Mavko et al. 2020). Also, the difference between results from KT and DEM models may be due to the amount of clay content in the samples from the Bakken formation, and this distinction could be better validated with Gamma Ray (GR) logs since GR is a proxy of clay content. However, in the GR logs from the Bakken formation, the upper and lower members of the Bakken formation have unusually high GR readings (Ostadhassan et al. 2012; Parapuram et al. 2017), but this might be further considered in other geologic formations.

Even though we only considered the effect of pore shapes and reservoir fluids (gas oil and water) on the seismic velocities and elastic moduli of the middle Bakken, there are other factors not considered in this paper that might also affect the seismic velocities and elastic moduli like pressure effect, effects of saturation with mixed fluids, partial saturation, and rocks with a mixture of pore shapes.

This study is however limited due to the non-availability of experimental data to correlate our numerical predictions of the fractomechanical properties.

5 Conclusions

In this study, the seismic velocities were correlated with a range of pore shapes, and the influence of pores shapes was investigated on the V_p and V_s, the relative effects of saturating fluids (gas, oil, and water) on the seismic waves. We assumed that different aspect ratios of pore morphology may be used to depict pore shapes. This was essential so that boundary conditions across defined surfaces are satisfied. Pore shapes are less regular in reality. It is evident from studies made with a scanning electron microscope that certain pores are rounded or vugular while others are flat. Cracks and extremely small grain boundary gaps play a significant part in regulating the elastic characteristics of rocks. The idea, although oversimplified, may consider these significant implications of pore shapes.

The major insights from this study are:

1. For a given matrix, increased porosity causes a drop in the elastic moduli and seismic velocities of rocks. The flatter pores have a considerably bigger impact on velocities than spherical pores for a given concentration of pores. If the aspect ratio of the pores is small enough, even in circumstances of extremely low porosity (less than 1% pores), the velocities would shift dramatically depending on the saturating fluids.
2. Shear velocities are often less affected by the properties of the saturating fluid than the compressional velocities. For all pore shapes, the gas-saturated case has lower bulk and shear moduli than the water- or oil-saturated case. Density dependency cause velocities to exhibit more complex behavior.
3. The gas-saturated case yields greater V_p and V_s for moldic pores than the water- or oil-saturated cases. Gas-saturated velocities are lower in pores that are penny-like shaped. For sedimentary rock models, V_s for gas-saturated rocks are either equal or greater (particularly for extremely porous rocks) than in dry or water-saturated cases. V_p for both cases are typically lower than for water-saturated cases.
4. V_p, V_s, and elastic moduli in Middle Bakken increase with a decrease in the porosity. The needle-like pores (crack) have a greater effect on V_p and V_s than the intergranular and intragranular pores depending on the saturating fluids.
5. In Middle Bakken, the V_p is more affected by the pore geometry than V_s depending on the density and properties of the saturating fluid. For all pore shapes considered, the gas-saturated case has smaller bulk and shear moduli than the oil- or water-saturated cases. In the lower aspect ratio (0.01) as opposed to the higher aspect ratio (0.2), the change in the bulk and shear moduli is more noticeable.
6. Lithofacies with needle-like pores (low aspect ratio) are more susceptible to fracturing than lithofacies with intragranular pores (high aspect ratio). This range of seismic velocities (V_p and V_s) with low aspect ratios is the target for hydraulic stimulation.
7. Middle Bakken has varying aspect ratios and varying pore morphology because of the distinctive lithofacies.
8. The middle Bakken formation will have a higher susceptibility to fracturing and faulting, and hence will achieve greater fluid (oil and water) recovery.
9. Specifically, the recommended lithofacies for lateral well landing for fracturing and reservoir

stimulation would be at lithofacies units 1, 2, and 4 because they have inherent low V_p and low aspect ratios.

Acknowledgements The financial support of the North Dakota Industrial Commission (NDIC) is acknowledged. We also appreciate the access to Bakken data from the North Dakota Industrial Commission website. We thank Ikon Science for the use of *RokDoc* software.

Declarations

Conflict of interest The authors declare that they have no conflict of interest.

Open Access This article is licensed under a Creative Commons Attribution 4.0 International License, which permits use, sharing, adaptation, distribution and reproduction in any medium or format, as long as you give appropriate credit to the original author(s) and the source, provide a link to the Creative Commons licence, and indicate if changes were made. The images or other third party material in this article are included in the article's Creative Commons licence, unless indicated otherwise in a credit line to the material. If material is not included in the article's Creative Commons licence and your intended use is not permitted by statutory regulation or exceeds the permitted use, you will need to obtain permission directly from the copyright holder. To view a copy of this licence, visit http://creativecommons.org/licenses/by/4.0/.

References

Anselmetti FS, Eberli GP (1999) The velocity deviation log: a tool to predict pore type permeability trends in carbonate drill holes from sonics and porosity or density logs. AAPG Bull 83:450–466. https://doi.org/10.1306/00AA9BCE-1730-11D7-8645000102C1865D

Avseth P, Dvorkin J, Mavko G, Rykkje J (2000) Rock physics diagnostic of North Sea sands: link between microstructure and seismic properties. Geophys Res Lett 27(17):2761–2764. https://doi.org/10.1029/1999GL008468

Avseth P, Mukerji T, Mavko G, Dvorkin J (2010) Rock-physics diagnostics of depositional texture, diagenetic alterations, and reservoir heterogeneity in high-porosity siliciclastic sediments and rocks: a review of selected models and suggested work flows. Geophysics. https://doi.org/10.1190/1.3483770

Azenkeng A, Mibeck BAF, Kurz BA, Gorecki CD, Myshakin EM, Goodman AL, Azzolina NA, Eylands KE, Butler SK, Sanguinito S (2020) An image-based equation for estimating the prospective CO_2 storage resource of organic-rich shale formations. Int J Greenh Gas Control 98(May):103038. https://doi.org/10.1016/j.ijggc.2020.103038

Berryman JG (1980a) Long-wavelength propagation in composite elastic media I. Spherical inclusions. J Acoust Soc Am 68(6):1809–1819. https://doi.org/10.1121/1.385171

Berryman JG (1980b) Long-wavelength propagation in composite elastic media II. Ellipsoidal inclusions. J Acoust Am 66(6):1820. https://doi.org/10.1121/1.385172

Berryman JG, Milton GW (1991) Exact results for generalized Gassmann's equations in composite porous media with two constituents. Geophysics 56(12):1950–1960. https://doi.org/10.1190/1.1443006

Biot MA (1956) Theory of propagation of elastic waves in a fluid-saturated porous solid. I. Low-frequency range. J Acoust Soc Am 28(2):168–191

Candikia YN, Rosid MS, Haidar MW (2017) Comparative study between Kuster–Toksoz and differential effective medium method for determining pore type in carbonate reservoir. AIP Conf Proc. https://doi.org/10.1063/1.4991289

Dvorkin J, Nur A (1996) Elasticity of high-porosity sandstones: theory for two North Sea data sets. Geophysics 61(5):1363–1370. https://doi.org/10.1190/1.1444059

Dvorkin J, Nur A, Chaika C (1996) Stress sensitivity of sandstones. Geophysics 61(2):444–455. https://doi.org/10.1190/1.1443972

Eshkalak MO, Aybar U (2015) Carbon dioxide storage and sequestration in unconventional shale reservoirs. J Geosci Environ Prot 3:7–15

Ferrill DA, McGinnis RN, Morris AP, Smart KJ, Sickmann ZT, Bentz M, Lehrmann D, Evans MA (2014) Control of mechanical stratigraphy on bed restricted jointing and normal faulting, eagle Ford Formation, south-central Texas. AAPG Bull 98:2477–2506. https://doi.org/10.1306/08191414053

Galvis H, Becerra D, Slatt R (2018) Lithofacies and stratigraphy of a complete Woodford Shale outcrop section in South Central Oklahoma: Geologic considerations for the evaluation of unconventional shale reservoirs. Interpretation 6(1):SC15–SC27. https://doi.org/10.1190/INT-2017-0074.1

Gassmann F (1951) Elastic waves through a packing of spheres. Geophysics 16(4):673–685. https://doi.org/10.1190/1.1437718

Gholizadeh Doonechaly N, Rahman SS, Kotousov A (2013) A new approach to hydraulic stimulation of geothermal reservoirs by roughness induced fracture opening. In: Bunger AP, McLennan J, Jeffrey R (eds) Effective and sustainable hydraulic fracturing. IntechOpen, London, pp 573–590. https://doi.org/10.5772/56447

Gudmundsson A, Simmenes TH, Larsen B, Philipp SL (2010) Effects of internal structure and local stresses on fracture propagation, deflection, and arrest in fault zones. J Struct Geol 32(11):1643–1655. https://doi.org/10.1016/j.jsg.2009.08.013

Handoyo, Fatkhan, Hutami HY, Sudarsana R (2019) Rock physics model to determine the geophysical pore-type characterization and geological implication in carbonate reservoir rock. IOP Conf Ser Earth Environ Sci. https://doi.org/10.1088/1755-1315/311/1/012031

Hilman J, Winardhi IS (2019) Rock physics template application on carbonate reservoir. IOP Conf Ser Earth Environ Sci. https://doi.org/10.1088/1755-1315/318/1/012006

Kashkooli SB, Gandomkar A, Riazi M, Tavallali MS (2022) The investigation of gas trapping and relative permeability alteration during optimization of CO_2-EOR and sequestration. Int J Greenh Gas Control. https://doi.org/10.1016/j.ijggc.2021.103529

Kolawole O (2022) Mechanistic study of microbial altered properties in dolostones. Rock Mech Rock Eng. https://doi.org/10.1007/s00603-022-03116-y

Kolawole O, Ispas I (2019) Interaction between hydraulic fractures and natural fractures: current status and prospective directions. J Pet Explor Prod Technol 10:1613–1634. https://doi.org/10.1007/s13202-019-00778-3

Kolawole F, Johnston CS, Morgan CB et al (2019) The susceptibility of Oklahoma's basement to seismic reactivation. Nat Geosci 12:839–844. https://doi.org/10.1038/s41561-019-0440-5

Kolawole O, Ispas I, Kumar M, Weber J, Zhao B, Zanoni G (2021a) How can biogeomechanical alterations in shales impact caprock integrity and CO_2 storage? Fuel 291:120149. https://doi.org/10.1016/j.fuel.2021.120149

Kolawole O, Ispas I, Kolawole F, Germay C, McLennan JD (2021b) Mechanical zonation of rock properties and the development of fluid migration pathways: implications for enhanced geothermal systems in sedimentary-hosted geothermal reservoirs. Geotherm Energy. https://doi.org/10.1186/s40517-021-00195-y

Kolawole O, Millikan C, Kumar M, Ispas I, Schwartz B, Weber J, Badurina L, Šegvić B (2022) Impact of microbial-rock-CO_2 interactions on containment and storage security of supercritical CO_2 in carbonates. Int J Greenh Gas Control 120(4):103755. https://doi.org/10.1016/j.ijggc.2022.103755

Kumar M, Han DH (2005) Pore shape effect on elastic properties of carbonate rocks: In: Society of exploration geophysicists: 75th seg international exposition and annual meeting, SEG 2005, no. January 2005, pp 1477–1480. https://doi.org/10.1190/1.2147969

Kuster GT, Toksöz NM (1974) Velocity and attenuation of seismic waves in two-phase media: part 1. Theor Formul 39(5):587–606

Laubach SE, Olson JE, Gross MR (2009) Mechanical and fracture stratigraphy. AAPG Bull 93:1413–1426. https://doi.org/10.1306/07270909094

LeFever JA, Martiniuk CD, Dancsok EFR, Mahnic PA (1992) Petroleum potential of the middle member, Bakken formation, Williston Basin. In: Proceedings of the sixth international williston basin symposium. Saskatchewan Geological Society Special Publication, pp 76–94. https://doi.org/10.1306/f4c900ce-1712-11d7-8645000102c1865d

Levin V, Markov M, Kanaun S (2004) Effective field method for seismic properties of cracked rocks. J Geophys Res Solid Earth. https://doi.org/10.1029/2003JB002795

Levine JS et al (2016) U.S. DOE NETL methodology for estimating the prospective CO_2 storage resource of shales at the national and regional scale. Int J Greenh Gas Control 51:81–94. https://doi.org/10.1016/j.ijggc.2016.04.028

Liu K, Ostadhassan M (2017) Microstructural and geomechanical analysis of Bakken shale at nanoscale. J Pet Sci Eng 153:133–144

Liu K, Ostadhassan M, Bubach B (2016) Applications of nanoindentation methods to estimate nanoscale mechanical properties of shale reservoir rocks. J Nat Gas Sci Eng 35:1310–1319

Lucia FJ (1999) Carbonate reservoir characterization. Springer, New York

Man CS, Huang M (2011) A simple explicit formula for the Voigt–Reuss–Hill average of elastic polycrystals with arbitrary crystal and texture symmetries. J Elast 105(1–2):29–48. https://doi.org/10.1007/s10659-011-9312-y

Markov M, Kazatchenko E, Mousatov A (2006) Compressional and shear wave velocities in multicomponent carbonate media as porosity functions. In: SPWLA 47th annual logging symposium 2006

Mavko G, Mukerji T, Dvorkin J (2020) The rock physics handbook. University Priniting House, Cambridge. https://doi.org/10.1017/9781108333016

McClure MW, Horne RN (2014) An investigation of stimulation mechanisms in enhanced geothermal systems. Int J Rock Mech Min Sci 72:242–260. https://doi.org/10.1016/j.ijrmms.2014.07.011

McGlade C, Speirs J, Sorrell S (2013) Unconventional gas: a review of regional and global resource estimates. Energy 55:571–584. https://doi.org/10.1016/j.energy.2013.01.048

Nojabaei B, Siripatrachai N, Johns RT, Ertekin T (2016) Effect of large gas–oil capillary pressure on production: a compositionally-extended black oil formulation. J Pet Sci Eng 147:317–329

Nordeng SH, Helms LD (2010) Bakken source system: three forks formation assessment. North Dakota Department of Mineral Resources, 22 p: April

Norris AN (1985) A differential scheme for the effective moduli of composites. Mech Mater 4(1):1–16. https://doi.org/10.1016/0167-6636(85)90002-X

Ostadhassan M, Zeng Z, Siavash Z (2012) Geomechanical modeling of an anisotropic formation-Bakken case study. In: 46th U.S. rock mechanics/geomechanics symposium, Chicago, Illinois

Ozotta O, Liu K, Ostadhassan M, Lee H, Pu H, Kolawole O, Malki ML (2021a) Time-dependent impact of CO_2-shale interaction on CO_2 storage. In: Proceedings of the 15th greenhouse gas control technologies conference

Ozotta O, Liu K, Gentzis T, Carvajal-ortiz H, Liu B, Ra S, Ostadhassan M (2021b) Pore structure alteration of organic-rich shale with Sc-CO_2 exposure: the Bakken formation. Energy Fuels. https://doi.org/10.1021/acs.energyfuels.0c03763

Ozotta O, Malki ML, Rasouli V, Pu H, Kolawole O (2021c) The effect of pore morphology on fracture systems. In: ARMA/DGS/SEG 2nd international geomechanics symposium, virtual, November 2021c

Ozotta O, Ostadhassan M, Liu K, Liu B, Kolawole O, Hadavimoghaddam F (2021d) Reassessment of CO_2 sequestration in tight reservoirs and associated formations. J Pet Sci Eng 206(June):109071. https://doi.org/10.1016/j.petrol.2021d.109071

Paoletti V (2012) Remarks on factors influencing shear wave velocities and their role in evaluating susceptibilities to earthquake-triggered slope instability: case study for the Campania area (Italy). Nat Hazards Earth Syst Sci 12(7):2147–2158. https://doi.org/10.5194/nhess-12-2147-2012

Parapuram GK, Mokhtari M, Hmida JB (2017) Prediction and analysis of geomechanical properties of the upper bakken shale utilizing artificial intelligence and data mining. In: SPE/AAPG/SEG unconventional resources technology conference

Pitman JK, Price LC, LeFever JA (2001) Diagenesis and fracture development in the Bakken formation. Williston Basin; Implications for reservoir quality in the middle member, 1653

Saberi MR (2020) Geology-guided pore space quantification for carbonate rocks. First Break 38(3):49–55. https://doi.org/10.3997/1365-2397.fb2020018

Saxena V, Michel K, Adam L (2018) Handbook of borehole acoustic and rock physics for reservoir characterization. Elsevier, Amsterdam

Senger K, Tveranger J, Braathen A, Olaussen S, Ogata K, Larsen L (2015) CO_2 storage resource estimates in unconventional reservoirs: insights from a pilot-sized storage site in Svalbard, Arctic Norway. Environ Earth Sci 73(8):3987–4009. https://doi.org/10.1007/s12665-014-3684-9

Singha DK, Chatterjee R (2017) Rock physics modeling in sand reservoir through well log analysis, Krishna–Godavari Basin, India. Geomech Eng 13(1):99–117. https://doi.org/10.12989/gae.2017.13.1.099

Slatt RM, Abousleiman Y (2011) Merging sequence stratigraphy and geomechanics for unconventional gas shales. Lead Edge 30:274–282. https://doi.org/10.1190/1.3567258

Sorensen JA, Braunberger JR, Liu G, Smith SA, Klenner RCL, Steadman EN, Harju JA (2014) CO2 storage and utilization in tight hydrocarbon-bearing formations: a case study of the bakken formation in the williston basin. Energy Procedia 63:7852–7860. https://doi.org/10.1016/j.egypro.2014.11.820

Toksöz MN, Cheng CH, Timur A (1976) Velocities of seismic waves in porous rocks. Geophysics 41(4):621–645

Ulmer-Scholle DS, Scholle PA, Schieber J, Raine RJ (2014) A color guide to the petrography of sandstones, siltstones, shales and associated rocks. AAPG memoir 109. American Association of Petroleum Geologists

Vernik L (2016) Seismic petrophysics in quantitative interpretation. Society of Exploration Geophysicists, Houston

Wang Q, Chen X, Jha AN, Rogers H (2014) Natural gas from shale formation: the evolution, evidences and challenges of shale gas revolution in United States. Renew Sustain Energy Rev 30:1–28. https://doi.org/10.1016/j.rser.2013.08.065

Wei J et al (2021) Experimental and simulation investigations of carbon storage associated with CO_2 EOR in low-permeability reservoir. Int J Greenh Gas Control. https://doi.org/10.1016/j.ijggc.2020.103203

Welkenhuyse K et al (2018) Economic threshold of CO_2-EOR and CO_2 storage in the North Sea: a case study of the Claymore, Scott and Buzzard oil fields. Int J Greenh Gas Control. https://doi.org/10.1016/j.ijggc.2018.08.013

Wyllie MRJ, Gregory AR, Gardner LW (1956) Elastic wave velocities in heterogeneous and porous media. Geophysics XXI(1):41–70

Xu J, Sonnenberg S (2016) Brittleness and rock strength of the Bakken formation, Williston basin, North Dakota. In: SPE/AAPG/SEG unconventional resources technology conference. OnePetro

Yan J, Li XY, Liu E (2002) Effects of pore aspect ratios on velocity prediction from well-log data. Geophys Prospect 50(3):289–300. https://doi.org/10.1046/j.1365-2478.2002.00313.x

Yu H, Ba J, Carcione J, Li JS, Tang G, Zhang XY, He XZ, Ouyang H (2014) Rock physics modeling of heterogeneous carbonate reservoirs: porosity estimation and hydrocarbon detection. Appl Geophys 11(1):9–22. https://doi.org/10.1007/s11770-014-0413-9

Publisher's Note Springer Nature remains neutral with regard to jurisdictional claims in published maps and institutional affiliations.